Heliyon

Influence of dewetting on the crystallization behavior of CuCl₂ in the presence of BSA during evaporation in a Petri dish

Nicolaas Busscher [a],[*],[1], Paul Doesburg [b], Gaby Mergardt [a], Anezka Sokol [a],[2], Johannes Kahl [a], Angelika Ploeger [a]

[a] *University of Kassel, Department of Organic Food Quality and Food Culture, Nordbahnhofstrasse 1a, D37213 Witzenhausen, Germany*

[b] *Crystal Lab, Kleefseweg 9, NL-6595 NK Ottersum, Netherlands*

[*] Corresponding author.

E-mail address: busscher@uni-kassel.de (N. Busscher).

[1] Present address: Sebastian Kneipp Strasse 44, D-37217 Witzenhausen, Germany.

[2] Present address: Brigadevej 40, 2300 København S, Denmark.

Abstract

The overall structure of dihydrate cupric chloride ($CuCl_2 * 2H_2O$) crystallization patterns in the presence of bovine serum albumin (BSA) in a Petri dish is influenced by dewetting. The dewetting behavior, which can be either before or after initial $CuCl_2$ nucleation, depends on the amount of $CuCl_2$ and BSA in the Petri dish. We postulate that the concentration and/or temperature gradient area in the dish, which is built up during the evaporation process, coincides with the location where dewetting predominantly starts. This hypothesis could be supported by measurements of the $CuCl_2$ coverage of the Petri dish. During the evaporation the height of the meniscus at the rim of the Petri dish recedes in favor of the central Petri dish area. This could not be explained by the above mentioned hypothesis.

Keywords: Molecular physics, Condensed matter physics

1. Introduction

The method of dihydrate cupric chloride with additives (shortly DCC crystallization method) comprises the evaporation and crystallization of DCC in the presence of an additive (the sample), resulting in additive-specific DCC patterns. These patterns can be characterized on the basis of different textural and structural features [1, 2]. The method has been applied in food research on different agricultural products and food samples such as apple juice [3], wheat [4, 5], milk [6], and carrots [7] Although there is still a lack of knowledge concerning the physical basis of the pattern formation process; e.g. for food authenticity tests [8]. Beckmann [9] and Leray [10] worked on the growth velocity, Leray [11] on the dendritic growth and a model for the profile of the solution, Gallinet [12] on the formation of a monolayer of Bovine Serum Albumin (shortly BSA) as additive including the process of dewetting and Holleman [13] and Busscher [14] on the evaporation profile. Busscher [15] defined a minimum set of physical parameters to research the basic processes during evaporation and crystallization that influence the overall structure of the DCC crystallization patterns, with and without the addition of additives.

Image analysis of DCC patterns grown in the presence of different additives revealed that the highest discrimination ability is located in a circular region of interest (ROI around the geometric center) of 30−70% of the Petri dish. Busscher [14] observed that -dewetting before crystallization- occurred in this area for the DCC-only case. The DCC patterns in the presence of different additives, ranging from single proteins to complex food matrices show -dewetting after crystallization- phenomena close to the rim of the Petri dish. These incomplete coverage of the surface close to the rim is clearly perceptible in DCC patterns with Polyvinylpyrrolidone (PVP) ([16]; Fig. 1), wheat [17] Fig. 5, and to a lesser extent with carrots [14, 15], as additives, but is absent for milk [16]. To study this process in more detail, BSA was chosen as additive
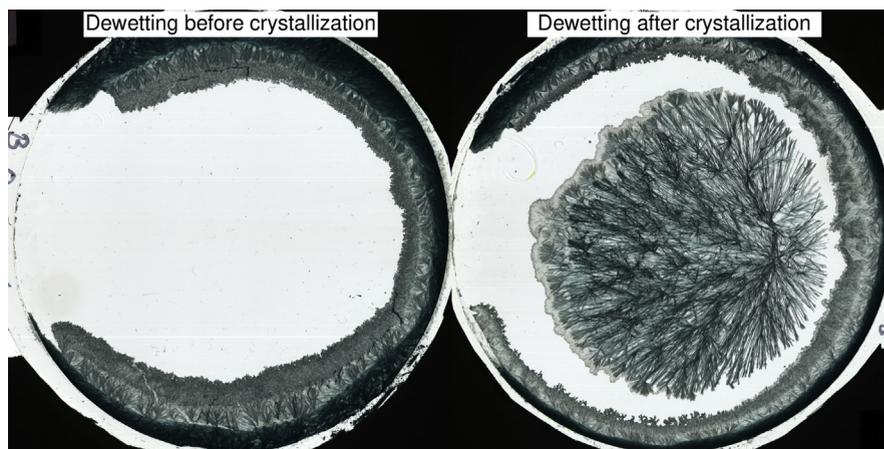
Fig. 1. Left, crystallization pattern of 600 mg DCC with dewetting before crystallization. Right, crystallization pattern of 600 mg DCC with dewetting after crystallization.

as it shows comparable limitations in the coverage of the surface [12] but is chemically and physically very well defined (e.g. with respect to surface effects and pH dependency) relative to the complex matrix of agricultural or food samples. Furthermore, BSA as additive considerably reduces the frequency of dewetting before crystallization compared to DCC only, resulting in more patterns available for evaluation. The dependency of the coverage of the Petri dish was studied for a range of mixing ratios of DCC and BSA.

2. Material and methods

2.1. Reagents and samples

Copper (II) chloride dihydrate (or dihydrate cupric chloride, shortly DCC) pro analysis was purchased from Merck (Ref. # 1.02733.1000). Bovine Serum Albumin (shortly BSA) was purchased from Sigma (Ref. # A2058). Samples were dissolved in bidest water (AppliChem/Germany, Order # 211074.0715). Vaseline was purchased from Sigma (Ref. # 16415).

2.2. Assembling the Petri dishes

The Petri dishes were assembled manually from circular glass-plates with a diameter of 10 cm and a thickness of 2 mm (Float-glas Pfähler/Germany) by mounting a 35 mm high acrylic ring with 9 cm inner diameter and a thickness of 5 mm. The connection between ring and glass-plate is supported by the addition of a thin layer of Vaseline. See for further details in [5, 7, 16].

2.3. Sample preparation

In each Petri dish a 6 ml volume was pipetted. For practical reasons the amounts of DCC and BSA are denoted in milligrams per plate, 600 mg DCC per plate corresponds to a 9.1 % weight solution, which equals 0.58 M (data from Koglin (1952) for 20 °C). 8.5 E-03 mg BSA per plate in a 6 ml volume amounts to 2.1 E-08 mM. The amount of BSA is also denoted in calculated monolayers per plate. The monolayers are calculated according to an estimated coverage of 83 +/-16 E-18 m^2 [18] per molecule, or 1.3 mg per m^2. This corresponds to 8.5 E-03 mg BSA per plate for a one monolayer build-up on a 9 cm diameter glass surface-area.

2.4. Evaporation conditions

A detailed description of the principles of the method is given by [5, 6], and [14]. Crystallization took place under controlled conditions with respect to temperature and relative humidity. Experiments were performed at a medium evaporation time until initial nucleation of 12−15 h at 30 °C and with 53% relative humidity at the

start above the Petri dishes. Dedicated software was used for laboratory and crystallization documentation. For each run 43 Petri dishes were crystallized.

2.5. Time-lapse stills

Time-lapse stills were made to follow the development of the dewetting and/or the crystallization by means of a Kodak DC5000 digital camera located at the ceiling of the crystallization chamber. Photographs with 2 MPixels resolution were taken every 10 minutes. Dewetting effects were observed by the visual evaluation of the photographs [14]. Details and fotos were shown in the supplementary information chapter 1.

2.6. Physical measurements

Density, pH and viscosity measurements for different mixing ratios of BSA and DCC made to model the evaporation process were performed by G. Mergardt. These mixing ratios consisted of a defined amount of BSA with increasing amounts of DCC until the solubility border was reached (See also chapter 2.1, supplementary information). Density was measured by means of an areometer (Alla Ateliers/ France), pH was measured with a ProLab1000 (Schott/Germany) with an EGA 143/PT100 Electrode (Meinsberg/Germany). Viscosity was measured with a DVII+ (Brookfield/Germany) with a specially manufactured coaxial-cylinder Teflon spindle (diameter 2.0 cm) to withstand the low pH (0.5) at high DCC concentrations. The spindle was calibrated with the certified viscosity standard oil B31 from Brookfield. Measurements were performed at 25.0 +/- 0.2 °C.

2.7. BSA adsorption calculations

When preparing low BSA concentrations (1−3 calculated monolayers) an estimation was made how much of the BSA in the solution would adsorb onto the glassware used to solubilize the BSA powder prior to pipetting into the Petri dish. According to [19] approximately 2.0 mg BSA/m^2 is lost due to random adsorption onto the glassware used to solubilize the BSA powder prior to pipetting into the Petri dishes. This loss would have a greater relative effect in the low BSA concentrations (1−3 calculated monolayer), and was therefore controlled for.

2.8. Scanning the crystallization patterns

Crystallization patterns were scanned in transparency mode with a UMAX Powerlook III scanner fitted with a UTA adapter. The LCh conversion was obtained with a IT8.7 reference Dia (Faust/Germany, Order #K3) and the little-cms software (from www.littlecms.com Version #1.15−1.1+etch3). Each scanned pattern was

connected to the documented information (temperature, humidity, evaporation and crystallization process) when pattern analysis was applied.

2.9. Transmission measurements

The pictures were scanned in transmission in RGB mode. To work with absolute and reproducible color values, the RGB values were transformed to L*C*h* by using a IT8 reference slide. The L* value is the luminescence value. When we neglect the reflection (and scattering) part, the transmission is approximately inverse proportional to the absorbance. The log of the absorbance would be -according to the Lambert Beer law- proportional to the thickness of the DCC needles. When we normalize the L* for a slice, as shown in Fig. SI.11, on the L* value for the whole picture, the slice with a radius from 80-100 % gives the percentage of the total DCC amount at the acrylic ring, where the meniscus is located.

2.10. Measurements on the coverage of the glass-plate with DCC crystals

The coverage of the glass-plate with DCC crystals is defined as the % coverage of the Petri-dish radius, starting at the geometric-center until the crystal-free region. See the supplementary information for more detailed information (Fig. SI.4).

3. Results

## 3.1. R1 Dewetting before and after crystallization of DCC without additives

In a previous paper [14] we observed dewetting of a DCC fluid film in the absence of additives. Dewetting occurs either before or after initial nucleation when during the evaporation phase the fluid layer thins to such an extent that the surface tension force exceeds the gravitational force. In the case of dewetting before initial nucleation, the dewetting process confines all the DCC to the rim of the glass-plate. Below a DCC amount of 600 mg/plate the probability of dewetting before crystallization increases proportionally.

Dewetting after crystallization can directly be observed from the time-laps stills documenting the evaporation/crystallization process at 600 mg DCC, because the contrast at this DCC concentration is high enough to distinguish between loss and retainment of integrity of the fluid film. The process of this type of dewetting can be described as follows (See also chapter 1.3 of the supplementary information): first, upon initial nucleation, the crystals start growing from a location near the geometrical center of the plate. During the growth of the crystals the intact fluid film is still visible on the time laps photos. When the primary crystal covers roughly

60 %−80 % of the dish surface, a solution free area appears, located between the centrally located primary crystal and the solution at the ring. Finally the solution at the ring starts crystallizing, culminating in two crystal areas separated by a crystal-free zone. This is visible in Fig. 1 on the right. In Fig. 1 on the left an example is presented of dewetting before crystallization.

3.2. R2 Dewetting before crystallization is inhibited by 1−3 monolayers of BSA

The hypothesis from Gallinet [12] was tested, which states that a minimum of one monolayer of BSA influences the dewetting behavior of a DCC solution. Hereto mixtures of varying amounts of DCC with BSA as additive were crystallized. For the evaluation of the dewetting process the same criteria as in [14] were used; either there is (1) dewetting before crystallization or there is (2) crystallization with or without dewetting during crystal growth (Fig. 1 right). In Fig. 2 the results are shown as a contour plot. The transition from (1) dewetting before crystallization to (2) crystallization before dewetting was observed for a DCC amount between 30 and 100 mg per plate, which more or less fits with the results from Busscher for the DCC only case [14]. Similarly this transition was observed for a BSA amount of about one to three calculated monolayers. Which is in good agreement with the hypothesis from Gallinet [12] and the estimation of the BSA losses due to adsorption onto the used glassware. The results show that for BSA values beyond three calculated
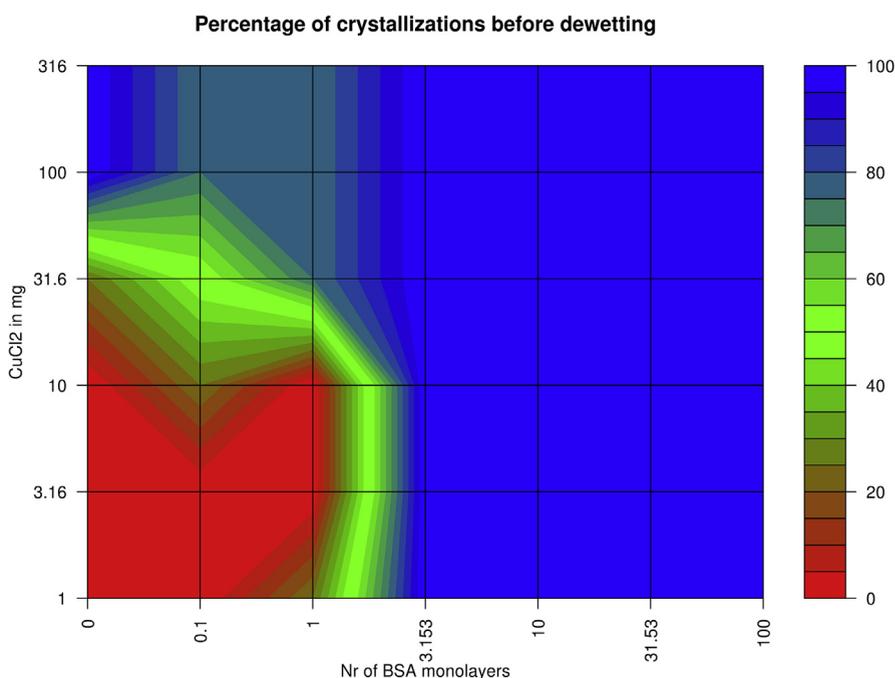
Fig. 2. Contour plot of the percentage of crystallization before dewetting (Z-Axis) for the DCC amount per plate (Y-axis) versus the BSA amount per plate (X-axis) shown as calculated mono-layers per plate.

monolayers dewetting before crystallization is prevented regardless of the DCC amount.

3.3. R3 Coverage of the plate, dependency on the BSA amount

### 3.3.1. Definition of the coverage of the Petri dish (ring3)

The coverage of the glass-plate with DCC crystals is quite different for the different DCC/BSA combinations. In order to quantify the coverage of the glass-plate, we measured the radius of the circular coverage with the primary DCC crystallization (% coverage of the Petri dish radius; see supplementary information chapter 2 for specific cases).

3.3.2. Recrystallization phenomenon, observation required for a clear measurement of ring3

A complicating factor in determining the circular coverage was revealed upon a closer observation of the DCC crystals. At DCC values of 177 mg and above, the peripherally located DCC coverage at the acrylic ring crystallizes later than the primary nucleation starting at the geometric center. Consequently, the peripherally located crystallization process partly overgrows the primary crystallization coverage. In Fig. 3 the cases for 10 mg DCC, 100 mg DCC and (with overgrowing from the rim) 316 mg DCC are represented. See also Fig. SI.3 for the time-lapse stills of this overgrowing phenomenon and Fig. SI.5 for a broader spectrum of DCC crystals with 177.6 monolayers of BSA in the supplementary information.

Therefore at DCC values where this overgrowing phenomenon emerges the circular coverage is restricted to the radius of the primary crystallization.

In Fig. 4 the dependency of the radius of the crystal coverage to the BSA amount is shown for a constant value of DCC. For 100 mg DCC per plate, the radius of the DCC coverage shows a sudden expansion from $60 - 90$ % in response to an increase
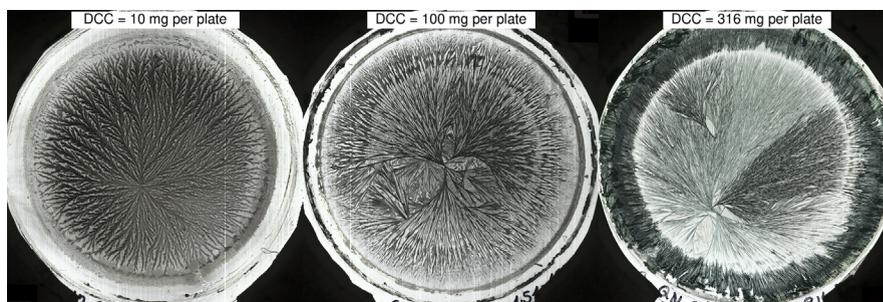
Fig. 3. Coverage of the plate for different amounts of DCC per plate. Left: 10 mg DCC per plate, middle 100 mg DCC per plate, right 316 mg DCC per plate. BSA additive amount was kept constant at 1.51 mg per plate (177.6 calculated monolayers).
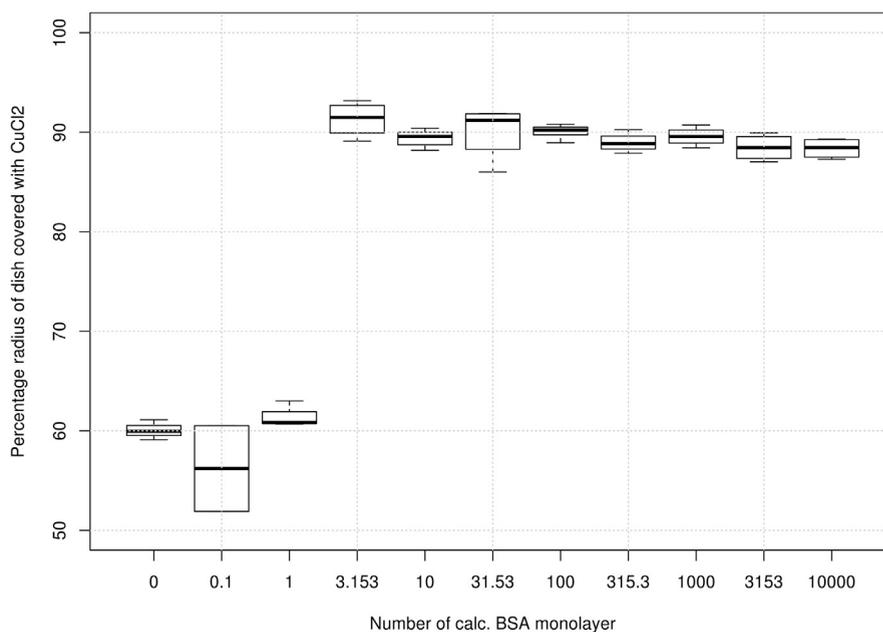
Fig. 4. Dependency of the radius of the DCC coverage of the plate (ring3_d) (Y-Axis, as percentage of the Petri dish radius) versus the BSA Amount (X-Axis) in calculated numbers of mono-layers for a DCC amount of 100 mg per plate.

in BSA amount from one to three calculated monolayers. After this sudden expansion the radius is slowly decreasing with increasing BSA amounts.

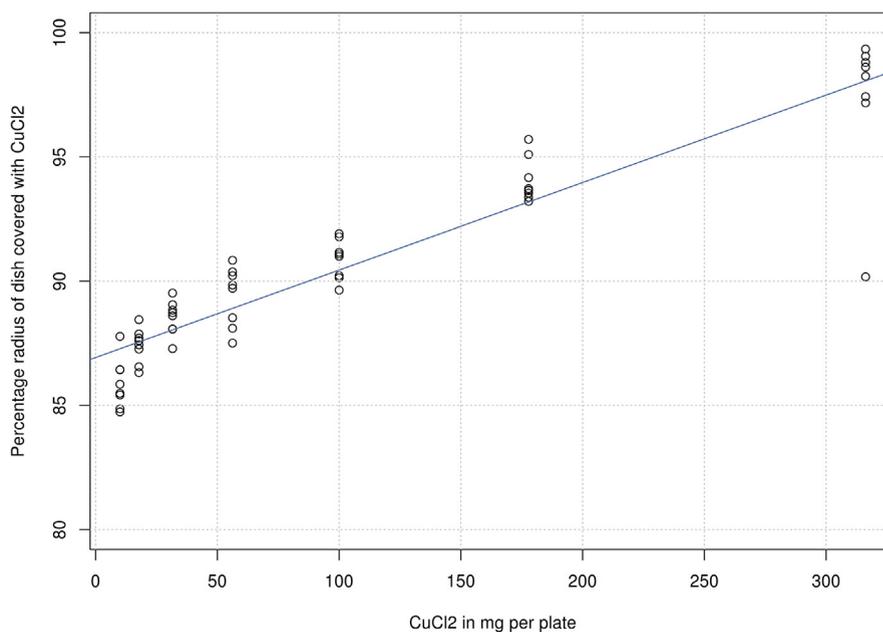## 3.4. R4 Coverage of the plate, dependency on the DCC amount

In Fig. 5 the dependency of the radius of the circular DCC coverage is plotted against increasing DCC amounts at a constant value of 177.6 calculated monolayers of BSA. There is a consistent increase of the radius in response to increasing DCC amounts.

3.5. R5 DCC amount on the ring; dependency on the DCC amount

Surprisingly, the percentage of the total DCC located at the periphery increases with an increasing amount of DCC per plate over the entire tested DCC-range. Whereas at the two lowest (shown) DCC values (10 and 17.7 mg per plate) no DCC deposit whatsoever was found at the periphery (Fig. 3, left for 10 mg DCC and Fig. SI.5 in the supplementary information for more DCC values and replicats).

3.6. R6 Transmission measurements

The observation in R5 could be substantiated by log(transmission) measurements of the scanned DCC crystals. This revealed additionally that the DCC amount at the acrylic ring is not only decreasing with a decreasing absolute amount of DCC, but

Fig. 5. Dependency of the radius of the DCC covered area in percentage of the Petri dish radius (ring_3d) (Y-axis) versus the DCC amount per plate (X-axis). BSA additive amount was kept constant at 1.51 mg per plate (177.6 calculated monolayers).

that this decrease is also a procentual decrease (see for Fig. SI.12 in chapter 4 of the supplementary information).

3.7. R7 BSA behavior during DCC crystallization

To observe whether the laboratory tests involving mixtures of BSA and DCC induced deviations from the DCC only behavior during the evaporation process, we measured the density, pH and viscosity for DCC with and without BSA and for comparison purposes also for DCC with PVP and DCC with Glycogen. The deviations from the DCC only behavior were quite small and, with respect to the viscosity, the conformational changes of BSA in reaction to the pH decrease were as expected (Yang and Foster, 1954). (See supplementary information chapter 3)

4. Discussion

Summarizing, we observed three types of DCC distribution in the Petri dish. They can be divided by the possible combinations of (a) DCC at the ring and (b) DCC around the geometric center and are shown in Fig. 6.

The cases in Fig. 6 are described with the conditions under which they appear and the possible hypothesis in Table 1.

Fig. 6. Three cases of distribution of DCC in the Petri dish. Left: DCC only at the periphery. Middle: DCC at the periphery and around the geometric center. Right: No DCC at the periphery, only around the geometric center.

Table 1. Case nr with type of pictures, their conditions and hypotheses.

Case	Type of picture	Conditions	Hypothesis
1	DCC only at the periphery	DCC only, no BSA	Dewetting before crystallization: H1
2	DCC at the periphery and around the geometric center	DCC only ≥ 31 mg or <31 mg DCC with BSA	Dewetting after crystallization: H1
3	No DCC at the periphery, only around the geometric center	low DCC (<31 mg) with BSA	?Dewetting from the ring?

4.1. Hypothesis 1 (H1)

Dewetting is promoted by an increasing overtension (see below) as a consequence of the evaporation process, and is triggered by a temperature- and/or concentration-gradient, which is built up during the evaporation. If nucleation occurs, the crystallization wave will amplify this trigger.

The type of dewetting by crystallization was described by [20] as a heterogeneous type of dewetting. Overtension is defined by the ratio of hcrit and hsol. Hcrit is the critical height where the surface tension and the gravity forces of the solution are in balance. Hsol is the height of the solution in the Petri dish at which the DCC solubility border is reached. Hsol is proportional to the DCC amount, hcrit is calculated according to [21] (see supplementary information chapter 1.3 table SI.1 for the formulas and the calculation results). Hypothesis H1 is in agreement with that postulated by [21], who connected dewetting to the height of the solution falling below Hcrit, creating a meta-stable situation. Additional disturbing factors, such as a surface tension gradient, were estimated to trigger dewetting.

4.1.1. Predictions from the hypothesis H1

Data from [14] indicates that in an area with radius 0−40 % around the geometric center of the Petri dish the conditions for concentration and temperature are more

or less comparable. From the existing measurement points in [14] it is clear that between a 40 %−80 % radius, a change takes place, indicative of a concentration gradient. [13] Shows that the dependency of the DCC concentration on the radius can be fitted by a parabolic curve, which would point to an increasing gradient towards the rim of the Petri dish. Based on this data predictions of hypothesis H1 are formulated, allowing a comparison with the results.

H1.1: At low degrees of overtension, the onset of dewetting will be located more towards the rim of the Petri dish, where the temperature and concentration gradients are higher.

H1.2: The probability of "dewetting before crystallization" is proportional to the degree of overtension (the overtension is higher at lower amounts of DCC, and at higher surface tensions).

H1.2a: As an extreme consequence of H1.2 the dewetting probability vanishes when the overtension becomes too low (at a high amount of DCC or a low surface tension in the Petri dish). As overtension is a prerequisite for dewetting, the trigger alone will not suffice in itself to initiate dewetting.

H1.3: A stronger trigger effect (a higher gradient, e.g. a combination from a concentration- and a temperature-gradient, or the presence of a crystallization wave) will result in the onset of the dewetting to be closer to the geometric center of the dish.

4.2. Case 1 in Table 1 (Dewetting before crystallization, DCC found only at the rim)

Result R1 discusses the crystallization before dewetting as in [14]. The prediction H1.1 states that the location of the onset of dewetting should be in an area with a radius above 40 %, where the gradients are found. At higher DCC amounts (i.e. lower degrees of overtension), the dewetting starting point should be located more towards the rim. In [14] it was reported that the location of dewetting was located more towards the rim than to the geometric center. The probability for dewetting before crystallization is growing with the decrease of the DCC amount, as shown in [14] and in R2 (case BSA amount = 0) which fits with prediction H1.2.

4.3. Case 2 in Table 1 (Dewetting after crystallization, DCC found at the rim and around the geometric center)

From R2 we could see that the coverage of the plate with a BSA amount > 1−3 calculated monolayers completely eliminates dewetting before crystallization. This means that hypothesis H1.2a is not only valid for a higher DCC amount but also for a lowering of the surface tension of the solution in the Petri dish.

When crystallization occurs before dewetting, then this can be regarded as an additional trigger for dewetting. In this case, according to prediction H1.3 the onset of dewetting is expected to be more independent of the gradient level. Consequently dewetting should initiate on average closer to the geometric center. This was not evaluated by a direct observation. But it was possible to be evaluated by the radius of the DCC crystal coverage in result R3. The coverage of the plate in Fig. 4 jumps from 1-3 monolayers of BSA from a radius of 60 % to a radius of 90 % (for 100 mg DCC per plate). As predicted in H1.1 a lower overtension (caused by the BSA monolayers) resulted in a more peripheral located onset of dewetting. The same became visible in R4, Fig. 5 where the lower overtension (caused by increasing DCC amounts) resulted in a consistent increase of the radius of the DCC crystal coverage.

4.4. Case 3 in Table 1. No DCC at the ring, DCC only found around the geometric center

For DCC amounts lower than 31 mg plate and for BSA amounts > three calculated monolayers the amount of DCC at the rim in % of the total amount of DCC is decreasing in response to decreasing DCC amounts. This implies that the amount of solution in the meniscus at the ring is decreasing during the evaporation. This is quit unexpected. To approach the problem the situation during the evaporation is described in detail.

During the evaporation the height of the solution decreases. We expect that the meniscus will follow the receding surface height of the solution. Firstly by a decrease of the contact angle to the receding angle, and secondly by following the surface height whilst maintaining the meniscus volume. The evaporation rate at the meniscus is lower than in the middle of the dish due to the shielding of the rim [13, 14]. Therefore the meniscus volume is expected to be less affected by the evaporation than the area around the geometric center, ruling the evaporation out as the reason for a decrease of the meniscus.

For all used DCC amounts the starting volume is 6 ml and the profile of the solution over the Petri dish is roughly the same at the start of the evaporation. The volume- and thus the height of the solution when reaching the DCC solubility border is decreasing with the DCC amount, which results in different profiles of the solution at the same solubility border for different DCC starting amounts.

In [14] the surface temperature of the solution was measured in the dish during the evaporation. The measurements for 60 mg and 600 mg DCC show after 10 hours of evaporation (1−2 hours before the start of the crystallization) a strong difference in the temperature gradient. In the case of 600 mg DCC per plate the temperature gradient was zero while for 60 mg DCC per plate the gradient was as strong as at the begin of the evaporation. The concentration gradient is still existing for 60

and for 600 mg DCC after 10 hours of evaporation [14]. When calculating the influence of the concentration- and the temperature-gradient on the surface tension gradient both have the same direction. A lower concentration (towards the rim) results in a lower surface tension. A higher temperature towards the rim (less evaporation) results in a lower surface tension. So both effects would increase the surface tension gradient as a trigger for dewetting.

With a higher overtension as a consequence of the lower DCC amount and a higher surface tension gradient towards the rim the location of the onset of dewetting should be more towards the geometric center (lower in % radius), which is in accordance with R4. This effect does however not explain why the volume of the meniscus is reducing. The % radius data points for the DCC amounts below 31 mg per plate are below the regression line in Fig. 5 (R4), which would fit with the above argumentation of a higher gradient due to the temperature gradient at low DCC amounts and the additional trigger by the crystallization wave, as was predicted in H1.3.

The reduction of the meniscus is a stepwise effect (R6) which points to an unknown factor in the process of dewetting by crystallization in the presence of gradients.

4.5. Summary of the discussion

For the hypothesis postulated in this article that dewetting is triggered by crystallization in an area with a concentration and a temperature gradient, three supporting and one thus far unexplained observations were found:

1. When adding BSA to a DCC solution, which subsequently lowers the degree of overtension, an increase in the radius of the DCC crystal coverage is found.

2. When increasing the DCC amount of the solution (in the presence of BSA), which lowers the overtension, an increase in the radius of the DCC crystal coverage is found.

3. When increasing the overtension of the solution (decreasing the DCC amount in the presence of BSA), the radius of the DCC crystal coverage of the plate is reduced.

4. However, for DCC amounts below 31 mg the decreasing DCC at the ring could not be explained by this hypothesis. This points to a missing parameter in the hypothesis.

5. Conclusions

The dewetting behavior of the crystallization of a DCC solution in the presence of BSA as additive in a Petri dish was researched. Based on the work from other authors [12, 20], a hypothesis could be formulated. The hypothesis postulates that the overtension (unbalance of surface and gravity forces in the solution) triggers dewetting in an area

where gradients of concentration or temperature exist. Crystallization amplifies the triggers. In support of the hypothesis three observations were found. One observation (the procentual reduction of DCC at the rim of the Petri dish) could not be explained and needs further research, because it seems to point to a hidden factor in the forces dealing with the dewetting in a Petri dish under the above described conditions.

Declarations

Author contribution statement

Nicolaas Busscher: Conceived and designed the experiments; Analyzed and interpreted the data; Contributed reagents, materials, analysis tools or data; Wrote the paper.

Paul Doesburg, Gaby Mergardt, Anezka Sokol: Performed the experiments; Analyzed and interpreted the data; Wrote the paper.

Johannes Kahl: Analyzed and interpreted the data; Wrote the paper.

Angelika Ploeger: Contributed reagents, materials, analysis tools or data; Wrote the paper.

Competing interest statement

The authors declare no conflict of interest.

Additional information

Supplementary content related to this article has been published online at https://doi.org/10.1016/j.heliyon.2018.e01102.

References

[1] J.O. Andersen, C.B. Henriksen, J. Laursen, A.A. Nielsen, Computerised image analysis of biocrystallograms originating from agricultural products, Comput. Electron. Agric. (22) (1999) 51–69.

[2] P. Doesburg, A.F. Nierop, Development of a structure analysis algorithm on structures from CuCl2·2H2O crystallization with agricultural products, Comput. Electron. Agric. (90) (2013) 63−67.

[3] J. Kahl, N. Busscher, P. Doesburg, G. Mergardt, F. Will, V. Schulzova, J. Hajslova, A. Ploeger, Application of crystallization with additives to cloudy and clear apple juice, Food Anal. Methods (10) (2016) 1−9.

[4] M. Szulc, J. Kahl, N. Busscher, G. Mergardt, P. Doesburg, A. Ploeger, Discrimination between organically and conventionally grown winter wheat farm pair samples using the copper chloride crystallisation method in combination with computerised image analysis, Comput. Electron. Agric. (74) (2010) 218−222.

[5] J. Kahl, N. Busscher, G. Mergardt, P. Maeder, T. Torp, A. Ploeger, Differentiation of organic and non-organic winter wheat cultivars from a controlled field trial by crystallization patterns, J. Sci. Food Agric. (95) (2014) 53−58.

[6] J. Kahl, N. Busscher, W. Hoffmann, G. Mergardt, I. Clawin-Raedecker, C. Kiesner, A. Ploeger, Development and performance of crystallization with additives applied on different milk samples, Food Anal. Methods (2013) 1−8.

[7] N. Busscher, J. Kahl, J.-O. Andersen, M. Huber, G. Mergardt, P. Doesburg, M. Paulsen, A. Ploeger, Standardization of the biocrystallization method for carrot samples, Biol. Agric. Hortic. (27) (2010) 1−23.

[8] E. Capuano, R. Boerrigter-Eenling, G. van der Veer, S.M. van Ruth, Analytical authentication of organic products: an overview of markers, J. Sci. Food Agric. (93) (2013) 12−28.

[9] H. Beckmann, Über Keimbildung, Einkristallwachstum und Auffächerungswachstum von CuCl2 * 2H2O in rein-wässerigen und Eiweiß-haltigen Lösungen, phdthesis, Universität Bonn, 1959.

[10] J.L. Leray, Growth kinetics of hydrated cupric chloride, J. Cryst. Growth (3-4) (1968) 344−349.

[11] J. Leray, Profile de la surface libre d'un film liquide heterogene, J. Chim. Phys. (10) (1973) 1428−1432.

[12] J.P. Gallinet, B. Gauthier-Manuel, Wetting of a glass surface by protein adsorption induces the crystallization of an aqueous cupric chloride solution, J. Colloid Interface Sci. 148 (1992) 155−159.

[13] L. Holleman, Ein Beitrag zum Verständnis der empfindlichen Kristallisation, Elem. Naturwissenschaft (4) (1966) 24−33.

[14] N. Busscher, J. Kahl, P. Doesburg, G. Mergardt, A. Ploeger, Evaporation influences on the crystallization of an aqueous dihydrate cupric chloride solution with additives, J. Colloid Interface Sci. (344) (2010) 556−562.

[15] N. Busscher, J. Kahl, A. Ploeger, From needles to pattern in food quality determination, J. Sci. Food Agric. (94) (2014) 2578−2581.

[16] J. Kahl, N. Busscher, W. Hoffmann, G. Mergardt, I. Clawin-Raedecker, A. Ploeger, A novel approach for differentiation of milk fractions and polyvinylpyrrolidone with different molecular weight by patterns derived from cupric chloride crystallization with additives, Anal. Methods (6) (2014) 3173−3176.

[17] J. Kahl, N. Busscher, G. Mergardt, A. Ploeger, Standardization and performance test of crystallization with additives applied to wheat samples, Food Anal. Methods (8) (2014) 2533−2543.

[18] J. Reynaud, I. Tavernier, L. Yu, J. Cochet, The adsorption of RNAse A, BSA and cytochrome c at the graphite powder|liquid interface using in parallel the adsorption isotherm plot and linear sweep voltammetry on graphite paste electrode, Bioelectrochem. Bioenerg. (15) (1986) 103−112.

[19] K. Nakanishi, T. Sakiyama, K. Imamura, On the adsorption of proteins on solid surfaces, a common but very complicated phenomenon, J. Biosci. Bioeng. (91) (2001) 233−244.

[20] M. Habibi, A. R, M. E, On dewetting of thin films due to crystallization (crystallization dewetting), Eur. Phys. J. E. 39 (2016) 30.

[21] A. Sharma, E. Ruckenstein, Dewetting of solids by the formation of holes in macroscopic liquid films, J. Colloid Interface Sci. (133) (1989) 358−368.